

NJC

Accepted Manuscript



This article can be cited before page numbers have been issued, to do this please use: U. Saha, M. Dolai and G. Suresh Kumar, *New J. Chem.*, 2019, DOI: 10.1039/C9NJ01018A.



This is an Accepted Manuscript, which has been through the Royal Society of Chemistry peer review process and has been accepted for publication.

Accepted Manuscripts are published online shortly after acceptance, before technical editing, formatting and proof reading. Using this free service, authors can make their results available to the community, in citable form, before we publish the edited article. We will replace this Accepted Manuscript with the edited and formatted Advance Article as soon as it is available.

You can find more information about Accepted Manuscripts in the [author guidelines](#).

Please note that technical editing may introduce minor changes to the text and/or graphics, which may alter content. The journal's standard [Terms & Conditions](#) and the ethical guidelines, outlined in our [author and reviewer resource centre](#), still apply. In no event shall the Royal Society of Chemistry be held responsible for any errors or omissions in this Accepted Manuscript or any consequences arising from the use of any information it contains.

Adaptable sensor for paying fluorometric detection of methanol molecules: theoretical aspects and DNA binding studies

Urmila Saha^{a,*}, Malay Dolai^b and Gopinatha Suresh Kumar^a

^aBiophysical Chemistry Laboratory, Organic and Medicinal Chemistry Division, CSIR-Indian Institute of Chemical Biology, 4, Raja S.C. Mullick Road, Kolkata 700 032, India.

^bDepartment of Chemistry, Prabhat Kumar College, Purba Medinipur 721404, West Bengal, India.

Abstract: The multifunctional Schiff base ligand N,N'-bis(5-nitro-salicylaldehyde)azine (NO₂-H₂SALNN) has been successfully synthesized and characterized by ESI-MS⁺, ¹H-NMR spectroscopy and CHN elemental analysis. The very feeble intrinsic fluorescence exerted by the ligand was found to be enhanced by several folds in the presence of methanol (~168 fold) and water (~10 fold) molecules. This enhancement of fluorescence intensity is supposed to be occurs as the result of blocking of rotational isomerization along the azomethine group (C=N) due to its coordination with solvent molecules, thereby exhibiting turn on fluorescence at two distinct wavelengths in presence of methanol and water having much difference of two emission wavelengths ($\Delta\lambda = 125$ nm). The hydrogen bond assisted enhancement fluorescence (HAEF) for methanol and water at two different wavelengths giving two different emissions may be due to the different size/nature of solvent as well as differences in solvent polarity. The binding of the NO₂-H₂SALNN and the solvent molecules were investigated and described by spectroscopic and computational studies. The bioactivity of NO₂-H₂SALNN has also been inspected by DNA binding measurements through spectrometric and thermodynamic studies. DNA binding studies reveal that the ligand interacts with double stranded CT-DNA through groove binding mode and the intrinsic binding constant was determined by calorimetric studies to be $(2.24 \pm 0.04) \times 10^5$ M⁻¹.

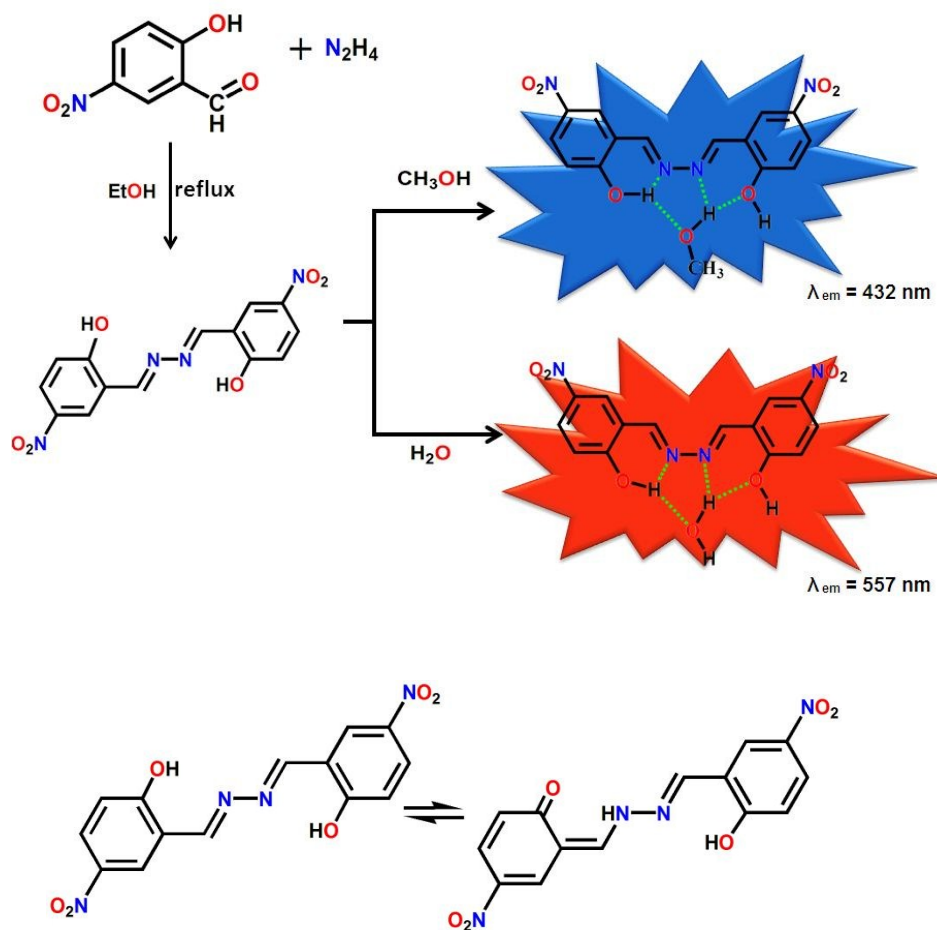
Introduction

In recent years, air pollution arising from volatile organic compounds (VOCs),¹⁻³ became a major environmental threat in Asian countries like Pakistan, Qatar, Afghanistan, Bangladesh, Egypt and India. VOCs are emitted from a variety of diffuse point sources, such as volatile solvent use, industrial wastes, urban water, accidental leaks, and from a wide array of daily used products, such as paints, fuels, petroleum products, raw materials, and solvents^{4,5}. Methanol is one of the hazardous VOCs, widely used for anti-freezing agents, paints, dyes, imitation spirits, and in automobiles, organic synthesis, wines for illegal profit⁶. Simultaneously, the common used artificial sweetener aspartame is converted to free methanol on hydrolysis of its 10% (by weight) molecules which is available for absorption⁷. Methanol is readily absorbed by inhalation, ingestion and dermal exposure. It is rapidly distributed to tissues through body water. A small amount of methanol is excreted unchanged by the lungs and kidneys. Methanol is metabolized primarily in the liver by sequential oxidative steps to formaldehyde, formic acid and carbon dioxide⁸. The initial step involves oxidation to formaldehyde by hepatic alcohol dehydrogenase. In step 2, formaldehyde is oxidized by formaldehyde dehydrogenase to formic acid/or formate depending on the pH. In step 3, formic acid is detoxified to carbon dioxide by folate-dependent reactions. Elimination of methanol from the blood via the urine, exhaled air and by metabolism appears to be slow in all species, especially when compared to ethanol.⁹ Swallowing, breathing, or absorbing large quantities of methanol through the skin, as in an industrial setting, can cause death.¹⁰ Exposure to methanol can cause visual problems and lead to blindness². Methanol can cause difficulty in breathing, lack of coordination, dermatitis, headache, dizziness, insomnia, confusion, nausea, vomiting, diarrhoea, inflammation of the pancreas, conjunctivitis, stomach problems and pain, weakness, leg cramps, and excessive sweating¹⁰. Hence, the effect of methanol from diffuse source is burning problem for human health and environments. Therefore, detection of methanol is very significant and relevant in this context, especially the selective sensing of methanol over other aliphatic alcohols.² Various organic luminescent fluorophores, Metal-organic frameworks, have received a great attention because of their potential applications in the detection of VOCs or metal ions by different spectroscopic studies^{10,11-15}. Though some Coordination polymers (CPs), lanthanides based Metal-organic frameworks

(MOFs) are reported for size-selective methanol detection, the use of simple organic moiety for the specific sensing of methanol is rare.

On the other hand, as DNA is the prime target for most of the drugs and small molecules, study of mechanism of interaction of small molecules with DNA and their chemotherapeutic effects have become an active research area at the interface of chemistry and molecular biology^{16, 17-19}. The major physicochemical tools for determinations of DNA are fluorescence and chemiluminescence^{20, 21}. Because of the non-fluorescent nature of DNA²², extrinsic fluorescent probes must be needed for the studies involving DNA.

Hence, we intended to design and synthesize a multifunctional organic fluorophore which may be proceed as a low cost regular used selective methanol sensor and also interacts with nucleic acids (DNA) in order that it can be used as DNA targeted drug in the near future. Accordingly, 2-hydroxy-5-nitro-benzaldehyde and hydrazine hydrate based Schiff base ($\text{NO}_2\text{-H}_2\text{SALNN}$) was synthesized and found to have weak intrinsic fluorescent, and it becomes a good probe for sensing methanol and water through hydrogen bonded assisted fluorescence enhancement (HAEF) at two different wavelengths, with enough difference of two emission wavelengths ($\Delta\lambda = 125 \text{ nm}$). We simultaneously assumed that the ESIPT and C=N isomerization may be disrupted upon hydrogen bonded coordination pair with methanol and water molecules that will solidify selective detection through spectral (UV-Vis and/ or Fluorescence) changes. The bioactivity of $\text{NO}_2\text{-H}_2\text{SALNN}$ has also been inspected by DNA binding measurements through spectrometric and thermodynamic studies.



Scheme 1: A schematic representation of preparation of hydrogen bonded coordination pair (above) and -C=N isomerisation of ligand (below).

Experimental Section

Materials and Methods

The starting materials such as hydrazine hydrate, 2-hydroxy-5-nitro-benzaldehyde (Sigma Aldrich) were used for the preparation of ligand. Calf thymus (CT) DNA (sodium salt, type XI, 42 mol% GC content), ethidium bromide (EB) and bisbenzimidazole (Hoechst 33258, ≥98% purity) were purchased from Sigma-Aldrich (St. Louis, MO, USA). All the buffer salts and other reagents were of analytical grade.

Physical measurements

Elemental analyses were carried out using a Perkin–Elmer 240 elemental analyzer. Infrared spectra (400–4000 cm⁻¹) were recorded from KBr pellets on Nicolet Magna IR 750 series-II FTIR spectrometers. ¹H-NMR was recorded in DMSO-d₆ on a Bruker 300 MHz NMR spectrometer. The absorption spectral titrations were performed on a Jasco V660 unit (Jasco International Co. Ltd., Hachioji, Japan) equipped with a thermoelectrically controlled cell holder and temperature controller in matched quartz cuvettes of 1 cm path length. Steady state fluorescence measurements were performed on a Shimadzu RF-5301PC fluorometer in fluorescence free quartz cuvettes of 1 cm path length.

Synthesis of Ligand (NO₂-H₂SALNN)

NO₂-H₂SALNN has been synthesised by refluxing 2-hydroxy-5-nitro-benzaldehyde (0.668g, 4mmol) and hydrazine hydrate (0.064 g, 2mmol) in ethanol for 4h (Scheme 1). The bright yellow solid amorphous compound deposited, which was collected by filtration and subsequent washing with water to free hydrazine. Yield, 80%; Melting point, 164°C; Anal. Calcd. for C₁₄H₁₀N₄O₆(330.25), C 50.92%, H 3.05%, N 16.96 %. Found: C 50.90%, H 3.10%, and N 16.98%. ¹H-NMR (Fig.S1, ES1⁺) (in DMSO-d₆) (δ, ppm): 7.43-7.89(6H), 8.93(s,2H), 11.16 (s, 2H(OH)).ESI-MS⁺ (m/z): 338.3224(NO₂-H₂SALNN +Li⁺+H⁺) (Fig.S2,ES1⁺).

Computational details

Ground state electronic structure calculations in gas phase of the ligand and its hydrogen bonded coordination pair with methanol (1) and water (2) have been carried out using DFT²³ method associated with the conductor-like polarizable continuum model (CPCM).²⁴Becke's hybrid function²⁵ with the Lee-Yang-Parr (LYP) correlation function²⁶ was used throughout the study. The absorbance spectral properties in MeOH/water medium were calculated by time-dependent density functional theory (TDDFT)²⁷ associated with the conductor-like polarizable continuum model. We computed the lowest 30 singlet – singlet transition and results of the TD calculations were qualitatively very similar.

For C, H, N, O atoms we employed 6-31+g as basis set for all the calculations.

The calculated electron-density plots for frontier molecular orbitals were prepared by using Gauss View 5.1 software. All the calculations were performed with the Gaussian 09W software package.²⁸ Gauss Sum 2.1 program²⁹ was used to calculate the molecular orbital contributions from groups or atoms.

DNA binding measurements

DNA samples were sonicated to uniform size of about (280 ± 50) base pairs in a Labsonic Sonicator (B. Brown, Germany) and were dialyzed under sterile conditions at 5 °C into the experimental buffer. The DNA sample exhibited characteristic ultraviolet absorption spectrum with an A₂₆₀/A₂₈₀ ratio between 1.88 and 1.92 and an A₂₆₀/A₂₃₀ ratio between 2.12 and 2.22. The concentration of the DNA was determined spectrophotometrically using a molar absorption coefficient value of 13,200 M⁻¹ cm⁻¹ expressed in terms of base pairs. All experiments were performed in filtered 10 mM citrate–phosphate (CP) buffer, pH 7.0 in deionized and triple-distilled water. All experiments were performed at 25±0.5°C. The biophysical experiments were carried out in 2% DMF–buffer (v/v) solution of the ligand NO₂-H₂SALNN.

The apparent binding affinity of DNA for the NO₂-H₂SALNN was determined by Absorbance and fluorescence spectral titration as described in our previous literature,^{16, 20, 30-34} the spectral titration data were analyzed by employing the Benesi–Hildebrand plot using modified Benesi–Hildebrand equation³³.

Hydrodynamic studies were carried out to check the binding mode of ligand with DNA. The details of hydrodynamic studies are described elaborately in the ESI.†

The competitive binding interaction between Hoechst 33258 and NO₂-H₂SALNN with DNA was performed by using fluorescence spectrophotometer^{20,32,34-36}. The concentration of DNA and Hoechst 33258 was 20 μM and 1.91 μM, respectively. Aliquots of stock solution of ligand (up to 0-20 μM) were added to the Hoechst 33258-DNA complex. Fluorescence spectra of the mixture were recorded at room temperature in the 400–670 nm using excitation wavelength of 350 nm.

Isothermal titration calorimetry experiments were performed on a VP-ITC microcalorimeter (MicroCal, Inc., USA, now Malvern Instruments, UK) to study the binding interaction of NO₂-H₂SALNN with DNA. Buffer solutions were degassed extensively prior to making the samples to prevent air bubble formation during titration. The data were analysed using Origin 7.0 software to obtain the thermodynamic parameters by following the protocols described in details previously^{19, 20, 31, 32, 34}. The heat associated with each injection was observed as a heat spike which is actually the measure of the power needed to maintain the sample and reference cells at same temperatures. The area under each peak was integrated to obtain the heat associated with that injection. Titrations were performed by injecting NO₂-H₂SALNN solution (125 μM) from the rotating syringe into the isothermal chamber containing 1.4235 mL of DNA solutions (60 μM) at 25 °C. The titration was performed in 28 sequential injections and each injection released 10 μL aliquots from the rotating syringe into the calorimeter cell. The corresponding dilution study of each reaction was performed in separate experiment by injecting identical volumes of the same concentration of the NO₂-H₂SALNN into the buffer alone. The heats of dilution were subtracted from the corresponding heat associated with the binding experiment that afforded the actual heat of NO₂-H₂SALNN-DNA interaction. The corrected injection heats were thereafter plotted as a function of the molar ratio and this was fitted with a model for one set of binding sites to calculate the equilibrium constant (K), the binding stoichiometry (N) and the standard molar enthalpy change (ΔH⁰) of association. The standard molar Gibbs energy change (ΔG⁰) was calculated using the standard relationship

$$\Delta G^0 = -RT \ln K \quad (2)$$

where *R* (1.9872041 cal K⁻¹ mol⁻¹) is the gas constant and *T* is the temperature in kelvins. Analysis of ITC data yielded the values of standard molar Gibbs energy and standard molar enthalpy change that enabled the calculation of TΔS⁰, where ΔS⁰ is the calculated standard molar entropy change, using the relationship

$$T\Delta S^0 = \Delta H^0 - \Delta G^0 \quad (3)$$

Results and Discussion

The ligand NO₂-H₂SALNN was synthesized by simple Schiff-base condensation between hydrazine and 2-hydroxy (5-nitro) benzaldehyde in ethanol (**Scheme 1**) and thoroughly characterized by ESI-MS⁺, ¹H-NMR spectroscopy and CHN elemental analysis.

Luminescent sensing of selective solvent molecules

UV–vis absorption spectrum of NO₂-H₂SALNN in DMF shows two intense absorption bands around 293 and 365 nm with a weak absorption band at 500 nm. With increasing the amount of methanol (MeOH:DMF (v/v) were 0.02, 0.04, 0.06, 0.08, 0.10, 0.12 and 0.14; keeping the total volume fixed at 2 ml and the concentration of NO₂-H₂SALNN constant at 20 μM) the absorbance of two peaks at 293 and 365 nm were found to get intensified with gradual decrease in the absorption peak at 500 nm (Fig. 1). Again, in presence of water (in the same experimental setup) a continuous decrease in the original band positions at 293 nm (with 9 nm hypsochromic shift) and 365 nm (with 12 nm bathochromic shift) was observed. These spectral changes may be due to the formation of a new species on increasing the concentration of Methanol or water. However in presence of other solvents (tetrahydrofuran, toluene, iso-propanol, n-butanol, and ethanol) in identical condition no significant changes in the absorption spectrum of NO₂-H₂SALNN were observed.

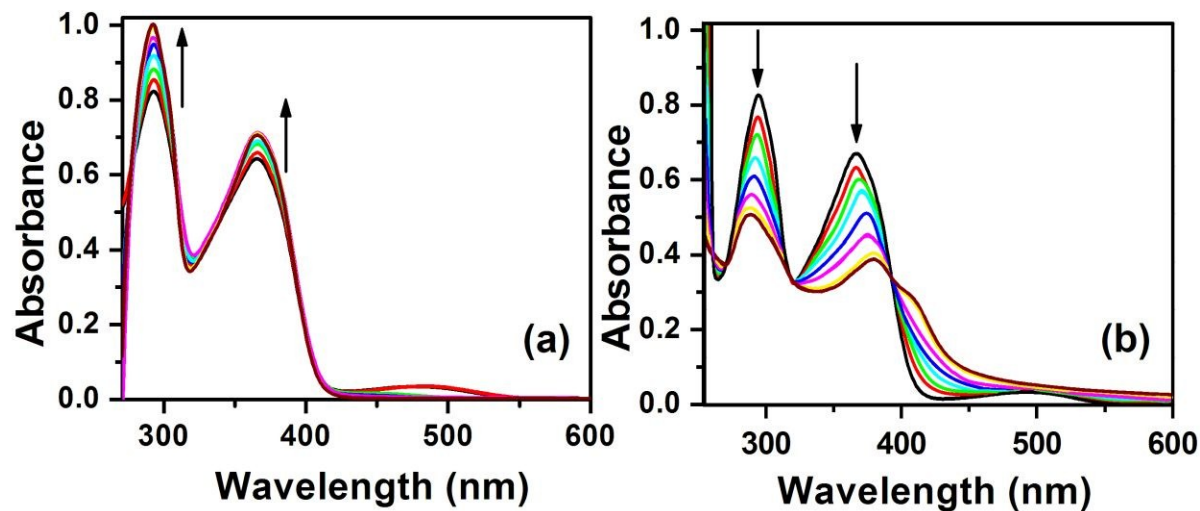


Figure 1. Absorption spectra of the receptor $\text{NO}_2\text{-H}_2\text{SALNN}$ ($20 \mu\text{M}$) in DMF with increasing concentration of methanol (a) and Water (b). (L:DMF (v/v) = 0.02, 0.04, 0.06, 0.08, 0.10, 0.12 and 0.14; where L stands for methanol or Water in respective cases)

The fluorimetric sensing experiment of $\text{NO}_2\text{-H}_2\text{SALNN}$ was carried out using several solvents THF, DMF, Toluene, water, methanol, ethanol, isopropanol and n-butanol. Fluorescence of the DMF solution of the receptor was tested by varying the DMF and other solvent ratio keeping the total volume and concentration ($20 \mu\text{M}$) fixed.

$\text{NO}_2\text{-H}_2\text{SALNN}$ itself showed very weak fluorescence at 560 nm on excitation at 375 nm. The receptor $\text{NO}_2\text{-H}_2\text{SALNN}$ exhibited excellent dual selectivity towards methanol and water in two different wavelengths at 432 nm and 557 nm respectively. However, the treatment of a DMF solution of the receptor $\text{NO}_2\text{-H}_2\text{SALNN}$ with methanol solvent resulted in a large (≈ 168 fold) increase in fluorescence intensity at a wavelength of 432 nm ($\Delta\lambda = 4$ nm) on excitation at 375 nm (Fig 2).

On the other hand the incremental addition of water to the $\text{NO}_2\text{-H}_2\text{SALNN}$ solution, increase the fluorescence intensity appeared at 557 nm ($\Delta\lambda = 3$ nm) with 10 fold enhancement of emission intensity on excitation at 375 nm (Fig 3).

The selective sensing of the probe is an important criterion of a successful sensor. In order to check the selectivity of the probe $\text{NO}_2\text{-H}_2\text{SALNN}$ towards methanol and water detection, we carried out fluorescence experiments with $20 \mu\text{M}$ of $\text{NO}_2\text{-H}_2\text{SALNN}$ and certain percentage of different solvent molecules.

To explore the binding affinity of $\text{NO}_2\text{-H}_2\text{SALNN}$ towards different solvent molecules viz. THF, DMF, Toluene, water, methanol, ethanol, isopropanol and n-butanol, the fluorescence spectral response of $\text{NO}_2\text{-H}_2\text{SALNN}$ was checked in the presence of each of these solvents in the same condition applied for both methanol and water addition titration. But these solvents except methanol and water remained inert towards sensing by the receptor $\text{NO}_2\text{-H}_2\text{SALNN}$ (Fig.4). We also checked the sensing selectivity of other aliphatic alcohols (ethanol, isopropanol and n-butanol) with $\text{NO}_2\text{-H}_2\text{SALNN}$ towards methanol (Fig.5). It is revealed that the blue fluorescence of $\text{NO}_2\text{-H}_2\text{SALNN}$ solution can be detected by using minimum 70% (v/v) of methanol in fluorescence spectra and 40% (v/v) of water detects the red fluorescence of $\text{NO}_2\text{-H}_2\text{SALNN}$ solution.

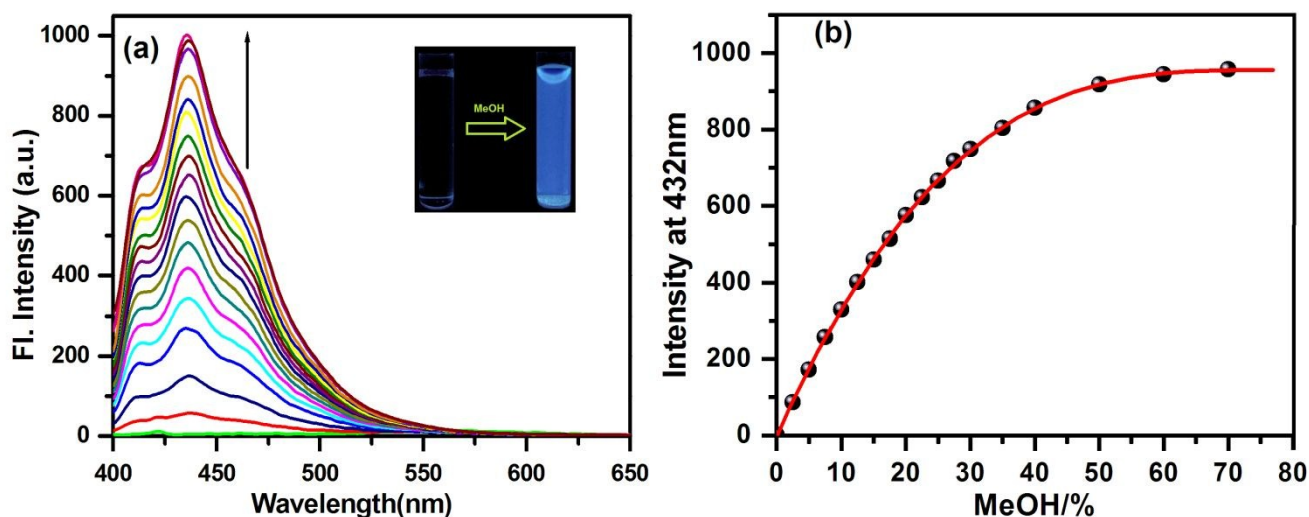


Figure 2. (a) Fluorescence spectra of the receptor $\text{NO}_2\text{-H}_2\text{SALNN}$ ($20 \mu\text{M}$) with methanol in DMF solution (b) Fluorescence intensity of the receptor $\text{NO}_2\text{-H}_2\text{SALNN}$ ($20 \mu\text{M}$) at 432nm as a function of % MeOH.

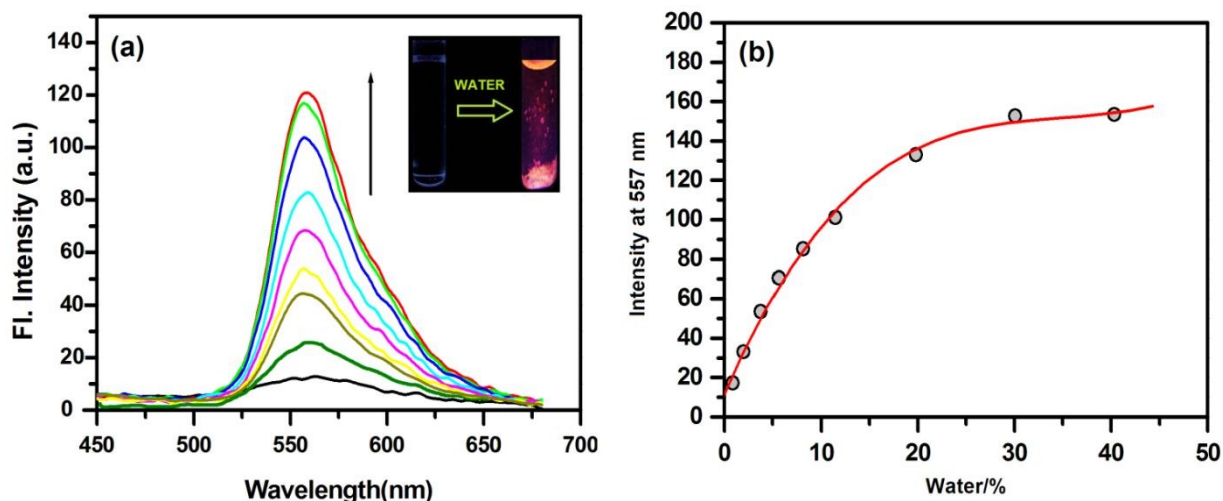


Figure 3. (a) Fluorescence spectra of the receptor $\text{NO}_2\text{-H}_2\text{SALNN}$ ($20 \mu\text{M}$) with water in DMF solution. (b) Fluorescence intensity of the receptor $\text{NO}_2\text{-H}_2\text{SALNN}$ ($20 \mu\text{M}$) at 557nm as a function of % H_2O pH-7.

The 1:1 stoichiometry for the hydrogen bonded coordination pair with methanol and water was confirmed by the HRMS spectra having the major peak located at 393.1846 and 349.1638 for the identified theoretical exact mass of the coordination pair **1** and coordination pair **2**.

Upon hydrogen bonded coordination pair with methanol and water with $\text{NO}_2\text{-H}_2\text{SALNN}$, a large HAEF (hydrogen bonding assisted enhanced fluorescence) effect is observed via 1:1 pair form which tends to produce a strong 'switch on' blue fluorescence for methanol corresponding an emission peak at 432 nm and red fluorescence for water with an emission peak at 557 nm. The HAEF induced fluorescence enhancement for methanol and water at two different wavelengths giving two different emissions color may be due to the different size/nature of solvent as well as the different polarity.

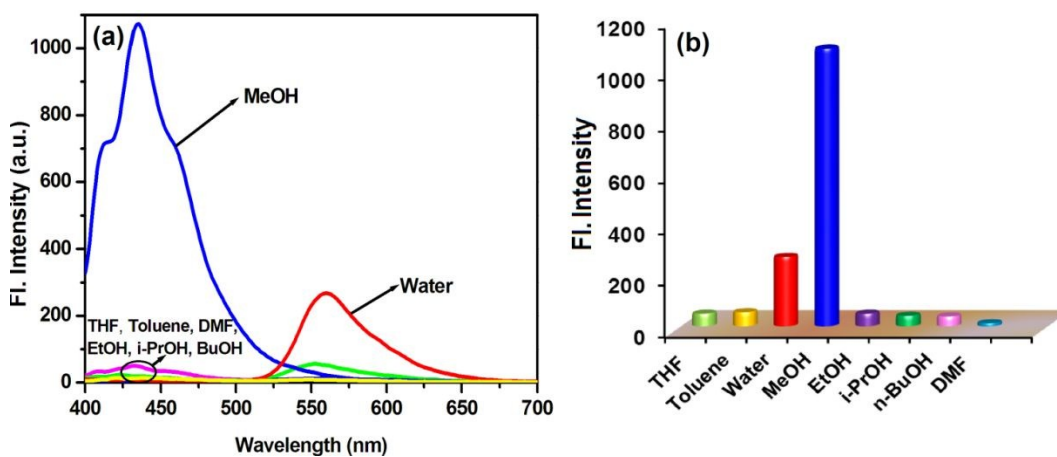


Figure 4. Fluorescence spectra of receptor $\text{NO}_2\text{-H}_2\text{SALNN}$ ($20 \mu\text{M}$) in DMF upon titration with 70% (v/v) of each of the different solvents at pH-7.

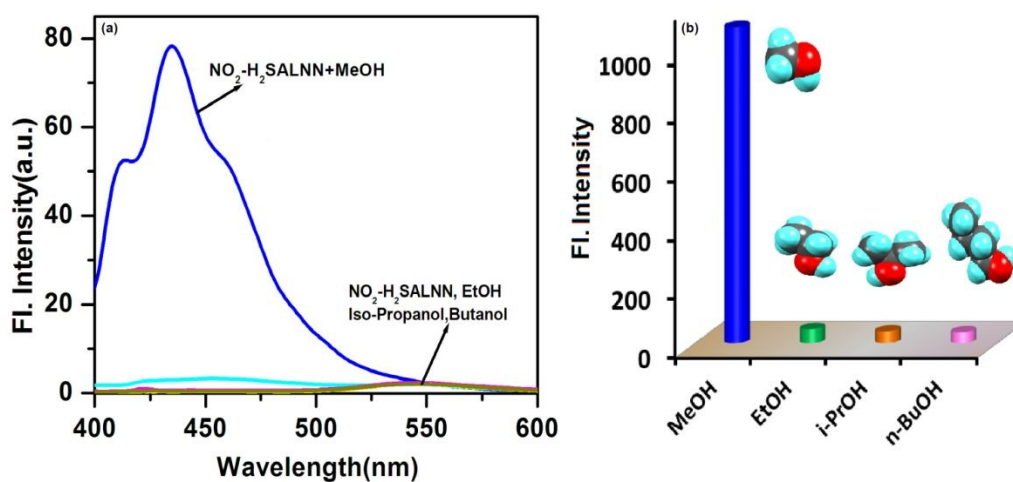


Figure 5. Fluorescence spectra of receptor $\text{NO}_2\text{-H}_2\text{SALNN}$ ($20 \mu\text{M}$) in DMF upon titration with 70% (v/v) of each of the different guest aliphatic alcohols at pH-7

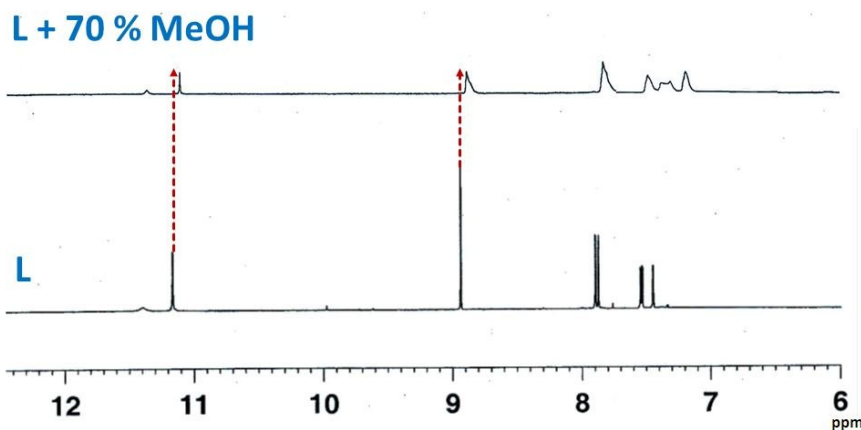


Figure 6. $^1\text{H-NMR}$ -titration spectra of ligand and its hydrogen bonded coordination pair with methanol.

Different spectroscopic techniques were adopted to establish the mode of coordination of NO₂-H₂SALNN probe towards MeOH and water ions in solution. The mass spectrum of [S(NO₂-H₂SALNN)] in DMF:MeOH=1:1(v/v), revealed a NO₂-H₂SALNN:S = 1:1 with ESI-MS⁺ (m/z) = 393.18 for ([NO₂-H₂SALNN...MeOH])+Na⁺+H⁺+Li⁺) and ESI-MS⁺(m/z) = 349.16 for ([NO₂-H₂SALNN...H₂O]+H⁺) (Fig. S3). A comparison of FTIR spectra of free NO₂-H₂SALNN, and their hydrogen bonded coordination pair revealed a shift in ν_{C=N} from 1662 cm⁻¹ for free ligand to 1633 and 1538 cm⁻¹ for methanol and water solvents, respectively indicating significant binding between them (Fig. S4- S6).

The coordination modes were further supported by ¹H-NMR studies (Fig. 6) which showed a change in chemical shifts of azomethine proton of the free ligand from 8.933 ppm to 8.914 ppm in the presence of 70% (v/v) methanol. The phenolic OH proton of the free ligand also showed a change in chemical shifts from 11.161 ppm to 11.169 ppm to its strong participation in hydrogen bonding to methanol but the other protons remains almost unchanged. So we can conclude that two phenolate-O and one imine-N of the receptor NO₂-H₂SALNN are involved in hydrogen bonding to methanol which was further supported by detail DFT calculations. The ¹H-NMR of ligand and water in DMSO-d₆ became hazy and didnot give any significant results.

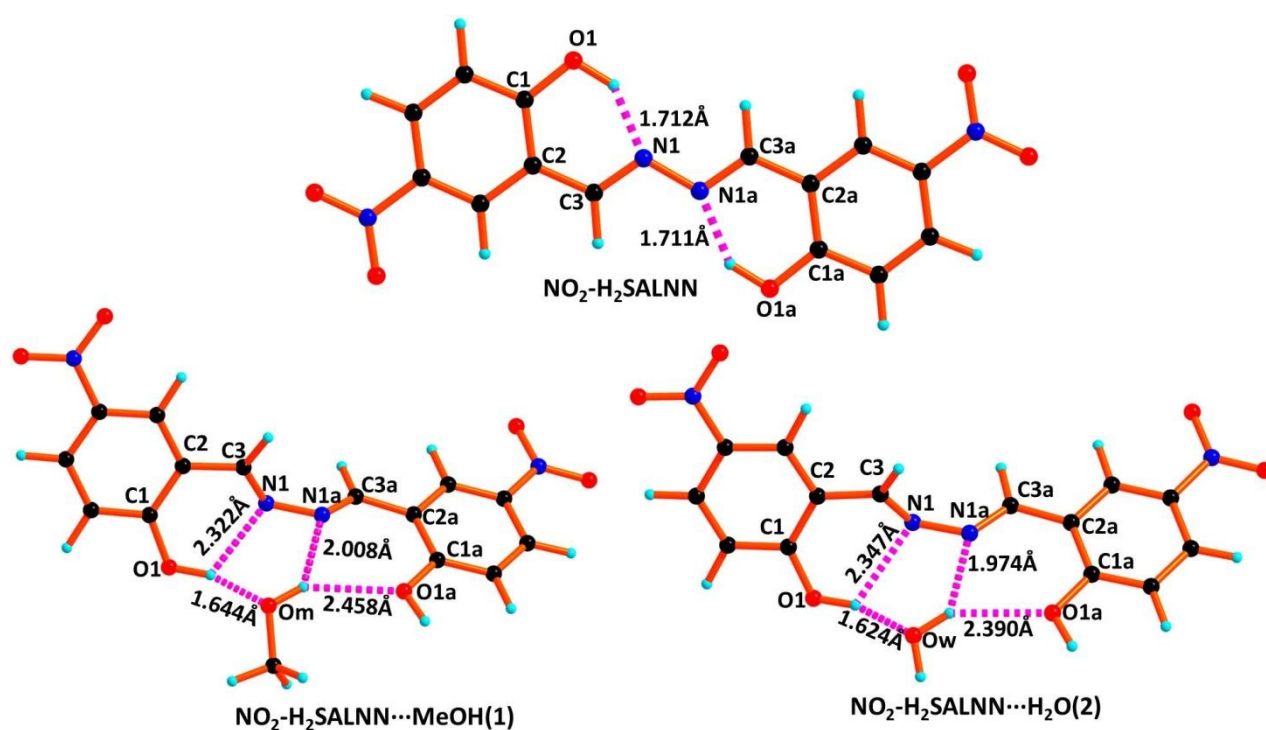


Figure 7. Geometry optimized molecular structures of target molecules (NO₂-H₂SALNN) and its hydrogen bonded coordination pair with methanol (1) and water (2).

Table 1. Selective bond distances and bond angles of **1** and **2**.

Bond distance(Å)	1	2	Bond angles(°)	1	2
N1-N1a	1.365	1.359	N1- O1H- O(sol)	85.80	85.12
N1...O1H	2.322	2.347	O1H- N1- N1a	114.28	112.66
N1a...O(sol)H	2.008	1.974	N1- N1a- O(sol)	87.88	89.11
O1...O(sol)H	1.644	1.624	N1a- O(sol)-O1a	75.17	76.88
O1a...O(sol)H	2.458	2.390	O1H- O(sol)-H	115.90	116.71

Table 2: The change of bond parameters in free ligand and **1** and **2**.

Bond distance(Å)	Free ligand	1	2
N1-N1a	1.402	1.365	1.359
C1-O1	1.354	1.349	1.349
C1-C2	1.430	1.431	1.432
C2-C3	1.445	1.461	1.462
C3-N1	1.307	1.291	1.291
C1a-O1a	1.354	1.381	1.382
C1a-C2a	1.430	1.420	1.420
C2a-C3a	1.445	1.461	1.459
C3a-N1a	1.307	1.292	1.292

Geometry optimization and electronic structure

The optimized geometries of NO₂-H₂SALNN and its hydrogen bonded coordination pair with methanol and water are shown in **Fig. 7**. The composition of the hydrogen bonded coordination pair with methanol and water are based on HRMS studies which displayed the presence of one methanol in **1** and one water in **2** as molecular fragment. Both coordination pairs have C1 point group. The important optimized geometrical parameters of them are listed in **Table 1**.

In the case of **1** and **2**, the ligand NO₂-H₂SALNN adopts hydrogen bonded coordination pair with methanol and water respectively. The hydrogen bonding distances are fall in the range 1.644-2.458Å and 1.624-2.390Å for **1** and **2**, respectively. The free ligand is optimized as *trans* form with respect to azo group and stabilized by hydrogen bond formation between phenolic-OH and azine nitrogens (1.711-1.712Å) whereas it adopts *cis* forms in **1** and **2** and therefore,

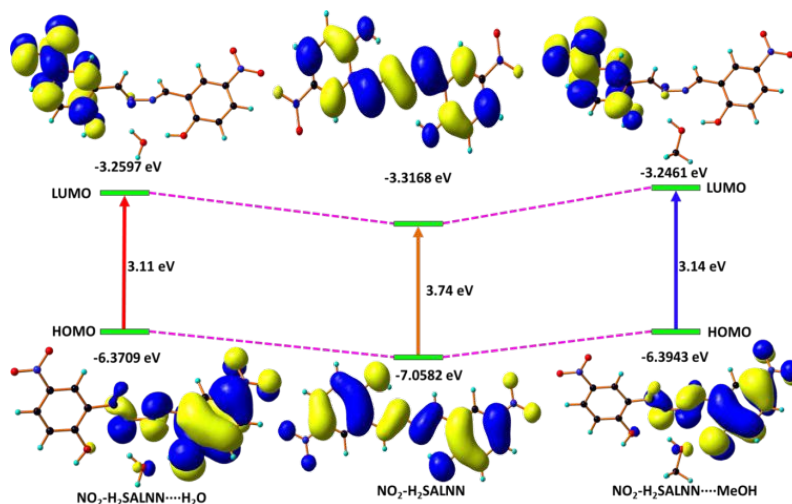


Figure 8. Frontier molecular orbital of $\text{NO}_2\text{-H}_2\text{SALNN}$ and $[\text{NO}_2\text{-H}_2\text{SALNN}\cdots\text{MeOH}](\mathbf{1})$ and $[\text{NO}_2\text{-H}_2\text{SALNN}\cdots\text{H}_2\text{O}](\mathbf{2})$ complex.

the changes in bond parameters along the azo bonds are listed in **Table 2**. The solvent molecules in **1** and **2** are capable to form bifurcated hydrogen bonding with ligand to give stable conjugate pairs.

In the case of $\text{NO}_2\text{-H}_2\text{SALNN}$ in the ground state, the electron density resides mainly on LUMO+1 and LUMO+2 orbital occurs at the phenyl ring and phenoxo oxygen along with nitro group, whereas the electron density on LUMO, HOMO, HOMO-1 and HOMO-2 orbital remains at $-\text{CH}=\text{N}$ along with phenoxo oxygen, and for HOMO-1 orbitals remains at azo-nitrogen atom with an energy gap between HOMO and LUMO of 3.74 eV (Fig. 8). In case of **1**, HOMO, HOMO-1 and HOMO-2 orbital mainly originates from the contribution of $-\text{CH}=\text{N}$ along with phenoxo oxygen and from methanol also and LUMO and LUMO+1 from phenoxo oxygen along with nitro group with an energy gap between HOMO and LUMO of 3.14 eV (Fig.7).

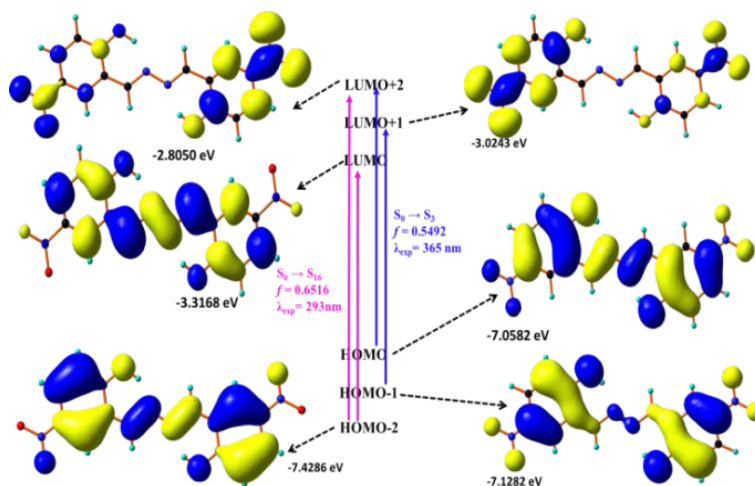


Figure 9. Frontier molecular orbitals involved in the UV-Vis absorption of the $\text{NO}_2\text{-H}_2\text{SALNN}$ in DMF solution.

In case of **2**, HOMO-1, LUMO+2 and LUMO+3 orbitals mainly originates from the contribution of total ligand part and HOMO, HOMO-2 and LUMO from mainly originates from the contribution of $-\text{CH}=\text{N}$ along with phenoxo oxygen and from water also with an energy gap between HOMO and LUMO of 3.11 eV (Fig. 8)

The UV-Vis absorption spectra of the ligands were studied at room temperature in DMF. The ligands showed two well resolved peaks at 365 and 293nm, respectively, and both are having ILCT character.

These bands are assigned to $S_0 \rightarrow S_3$ and $S_0 \rightarrow S_{16}$ electronic transitions, respectively (Fig. 9). The absorption energies associated with their oscillator strengths are given in Table 3a.

On the other hand, **1** shows two absorption bands at 365 and 293 nm (Fig. 10) in MeOH at room temperature and

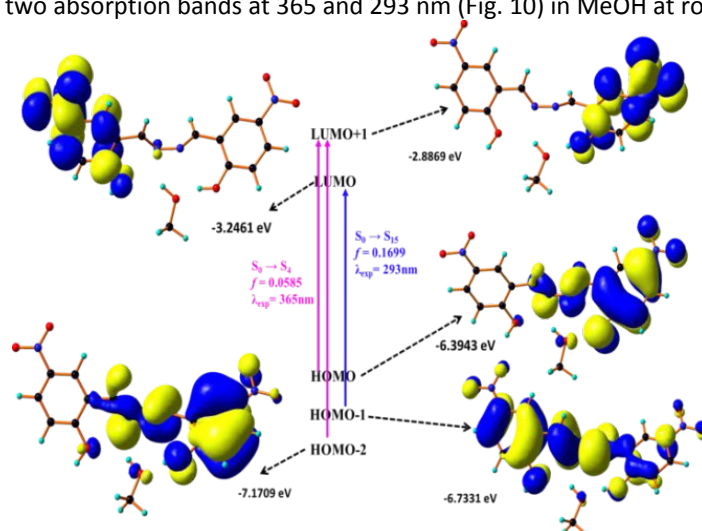


Figure 10. Frontier molecular orbitals involved in the UV-vis absorption of complex **1**.

the corresponding calculated absorption bands are located at 360.2 and 292.9nm which are in excellent agreement with experimental results (Table 3b). These two absorption bands can be assigned to the $S_0 \rightarrow S_4$ and $S_0 \rightarrow S_{15}$ transitions, respectively (Fig.10) originating from ILCT transitions.

The conjugate **2** shows two absorption bands at 379 and 288nm (Fig. S1) and the corresponding calculated absorption bands are located at 385.7 and 292.35nm which are in excellent agreement with experimental results (Table 3c). These absorption bands can be assigned to the $S_0 \rightarrow S_3$ and $S_0 \rightarrow S_{15}$ transitions respectively originating from ILCT transitions.

DNA binding studies

Absorbance and Fluorescence Spectral Studies

UV-visible absorption spectroscopy is a very popular method to detect the interaction of small molecules with DNA and formation of their complexes. Commonly, when a small molecule interacts with DNA and form a complex, changes in the absorbance and/or shift in the position of peaks are observed³⁷. The strength of interaction is correlated with the magnitude of changes in the absorbance or shifting in the peak position. The binding constant of $\text{NO}_2\text{-H}_2\text{SALNN}$ with DNA was estimated by monitoring the absorption band around 380 nm, where the absorbance of DNA is negligible. The absorption titration spectra of $\text{NO}_2\text{-H}_2\text{SALNN}$ exhibited 47% hypochromicity of the peak at 380 nm upon addition of increasing concentrations of DNA (Fig. 11a).

$\text{NO}_2\text{-H}_2\text{SALNN}$ showed an emission maximum at 557 nm upon excitation at 375 nm. The interaction was studied by titrating a constant concentration of $\text{NO}_2\text{-H}_2\text{SALNN}$ (20 μM) with increasing concentration of DNA. In presence of increasing concentration of DNA, a decrease in the fluorescence intensity of $\text{NO}_2\text{-H}_2\text{SALNN}$ was observed without any shift in the emission maximum (Fig. 11b). This lessening in the fluorescence intensity upon binding to DNA suggested an effective interaction of the ligand $\text{NO}_2\text{-H}_2\text{SALNN}$ with DNA.

The spectral data obtained from absorbance and fluorescence titration studies were used to build Benesi-Hildebrand plots to determine the apparent equilibrium constant (K_{BH}) for $\text{NO}_2\text{-H}_2\text{SALNN}$ -DNA complexation. The ratio of the intercept to slope afforded the apparent equilibrium constant as described in our previous literature^{16, 20, 30-34}. From spectrophotometry, the magnitude of the apparent equilibrium constant was deduced to be $(2.14 \pm 0.07) \times 10^5 \text{ M}^{-1}$. Similarly, from spectro-fluorimetry the value of K_{BH} was estimated to be $(2.26 \pm 0.04) \times 10^5 \text{ M}^{-1}$. It can be seen that these two values, obtained from spectrophotometry and fluorimetry, were in close agreement with each other.

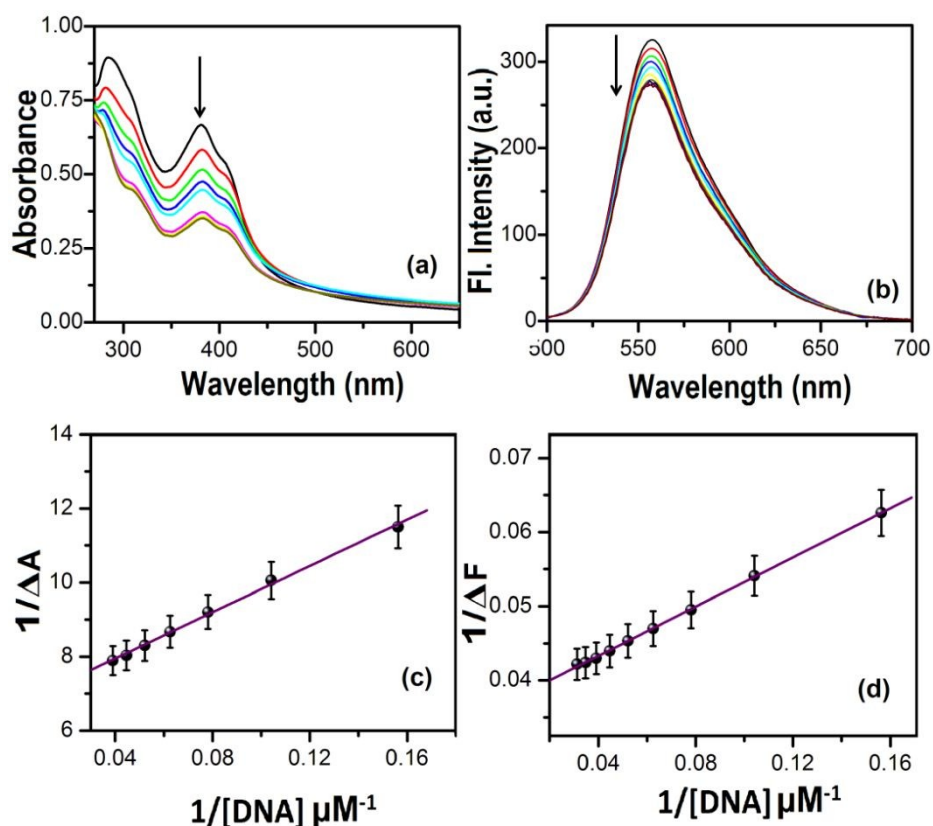


Figure 11. (a) Absorbance and (b) Fluorescence titration profile of $\text{NO}_2\text{-H}_2\text{SALNN}$ ($20 \mu\text{M}$) in the presence of increasing concentration of CT DNA [$0\text{-}26 \mu\text{M}$]; Modified Benesi–Hildebrand plots from (c) absorbance and (d) fluorescence titration data are shown in inset. Excitation wavelength was 375 nm .

Hydrodynamic studies

The mode of binding of $\text{NO}_2\text{-H}_2\text{SALNN}$, to DNA was further investigated by viscosity measurements. Hydrodynamic method provides unequivocal evidence in ascertaining DNA binding mode of small molecules in solution. Upon intercalation the axial length of the DNA increases and it becomes more rigid. Both factors increase the frictional coefficient and hence the viscosity of DNA in solution^{16, 20, 30-34}. In contrast, groove or surface binding causes a decrease in the effective length of DNA leading to a minor decrease in the relative viscosity of the DNA solution. The viscosity of the DNA solution was estimated in the presence of increasing concentrations of $\text{NO}_2\text{-H}_2\text{SALNN}$, and the change in the relative viscosities with increasing D/P values was calculated. The relative viscosities of the DNA solution (Fig. S7), showed only negligible change in the presence of $\text{NO}_2\text{-H}_2\text{SALNN}$. Such minor changes in relative viscosity may be correlated to a groove binding model.

Determination of the binding mechanism by Hoechst 33258 displacement assay

In order to provide further insights into the mode of binding of $\text{NO}_2\text{-H}_2\text{SALNN}$ with DNA, a displacement assay was performed by using Hoechst 33258 as a probe. Hoechst 33258 is a synthetic N-methylpiperazine derivative, which shows a specific binding affinity for the A–T rich sequences located along the minor grooves of DNA^{38,39}. The enhancement of the fluorescence intensity is usually ascribed to the higher planarity of the N-methylpiperazine derivative when bound to ds-DNA as well as to its protection from collisional quenching³². If $\text{NO}_2\text{-H}_2\text{SALNN}$ competes for the same DNA binding sites of Hoechst, a decrease of the fluorescence intensity of the latter must be observed. As depicted in Fig. 12, the fluorescence of the Hoechst–DNA complex is efficiently reduced ($\approx 93\%$) by the addition of $\text{NO}_2\text{-H}_2\text{SALNN}$. This observation is strongly pointing out the ability of $\text{NO}_2\text{-H}_2\text{SALNN}$ to displace Hoechst from the adenine and thymine binding sites located in the minor groove.

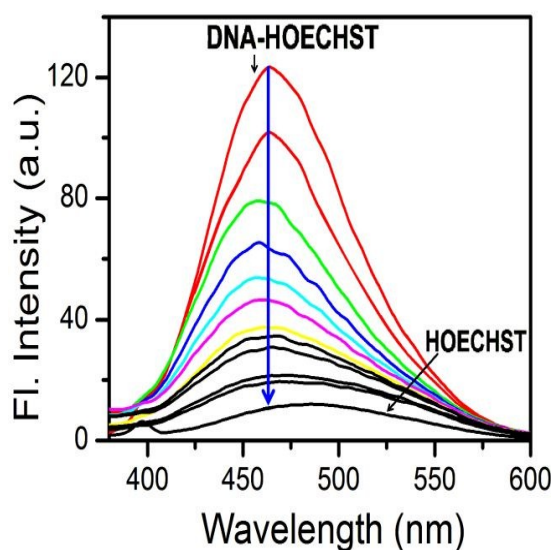


Figure 12. Fluorescence emission spectra of the competition between the Hoechst–DNA complex (λ_{exc} : 350 nm) and $\text{NO}_2\text{-H}_2\text{SALNN}$ (0.0–26 μM). $C_{\text{Hoechst}} = 1.91 \mu\text{M}$ and $C_{\text{DNA}} = 20 \mu\text{M}$.

Isothermal titration calorimetry studies of DNA-MTA interaction

Isothermal titration calorimetry (ITC) is a highly sensitive and reliable technique for studying the interaction of metal complexes with DNA that can precisely yield values of various thermodynamic quantities along with the binding affinity and stoichiometry of the interaction^{19, 20, 30, 32}. A single ITC experiment can yield all values of thermodynamic parameters like equilibrium constant (K), the stoichiometry (N), standard molar enthalpy (ΔH^0), standard molar Gibbs energy (ΔG^0), and standard molar entropy of binding ($T\Delta S^0$). In order to gather an in-depth knowledge on the binding of $\text{NO}_2\text{-H}_2\text{SALNN}$ to DNA, isothermal titration calorimetry study was performed. Fig. 12 depicts the calorimetric profile for the titration of $\text{NO}_2\text{-H}_2\text{SALNN}$ into the DNA solution at 298.15 K. The thermogram revealed exothermic interaction with a single binding event. The exothermicity of the reaction is evident from negative peaks in the plot of power versus time (upper panels of Fig. 13). The binding constant was deduced to be $(2.31 \pm 0.04) \times 10^5 \text{ M}^{-1}$ which is in close agreement with the binding constant values obtained from the spectroscopic analysis. The stoichiometry value (N) was found to be 0.43. The site size value (n) is defined as the reciprocal of the stoichiometry value (N). In our case, the value of n comes out to be 2.32. The binding was favored by negative enthalpy and positive entropy changes. The standard enthalpy and entropy values as determined from ITC are $-2.249 \text{ Kcal mol}^{-1}$ and $18.3 \text{ cal mol}^{-1}$, respectively. The value of ΔG^0 was determined by the expression, $\Delta G^0 = \Delta H^0 - T\Delta S^0$. This Gibbs energy value was $-7705.14 \text{ cal mol}^{-1}$.

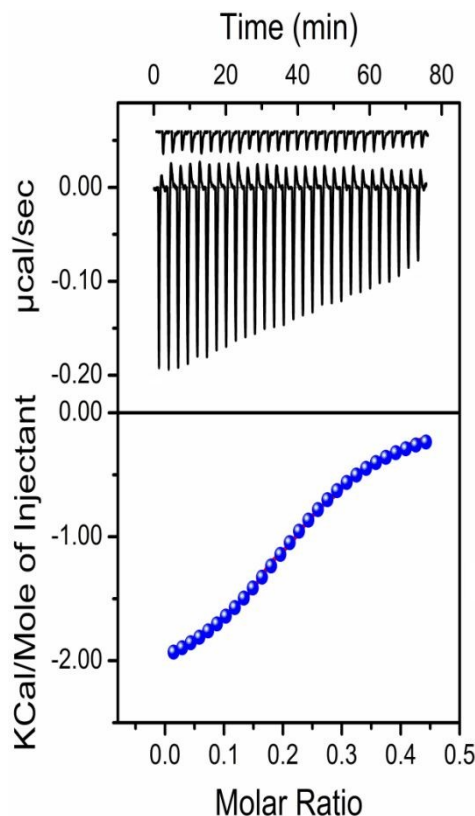


Figure 13. ITC profile for the titration of $\text{NO}_2\text{-H}_2\text{SALNN}$ with CT-DNA at $T=298.15$ K. The top panel represents the raw data resulting from the sequential injection of $\text{NO}_2\text{-H}_2\text{SALNN}$ into CT-DNA solution and the lower panel represents the corresponding normalized heat signals versus molar ratio. The data points (\bullet) are the experimental injection heats while the continuous line is the best fit curve to the experimental data using single binding sites model. The concentration of CT-DNA in the calorimeter cell was $60 \mu\text{M}$ and aliquots of $\text{NO}_2\text{-H}_2\text{SALNN}$ ($125 \mu\text{M}$) were titrated.

Conclusions

The multifunctional ligand N,N' -bis(5-nitro-salicylaldehyde)azine ($\text{NO}_2\text{-H}_2\text{SALNN}$) has been synthesized and characterized by various spectroscopic techniques. This free ligand becomes very weakly fluorescent due to the *cis/trans* isomerization along C=N bond of the azomethine group at excited state. But when it is used as a probe it ($\text{NO}_2\text{-H}_2\text{SALNN}$) exhibits differentially selective turn on sensing for methanol and water at two different wavelengths giving two different emissions colour may be due to the different size/nature of solvent. The coordination modes of the ligand-solvent complexes were investigated by spectroscopic and computational studies. Furthermore, we have studied the interaction of the ligand with CT-DNA by spectroscopic and calorimetric techniques which showed that $\text{NO}_2\text{-H}_2\text{SALNN}$ binds with CT-DNA through groove binding mode. Displacement studies confirmed that it interacts with double stranded DNA at the adenine and thymine (A-T) binding sites located in the minor groove. The calorimetric technique further confirms the spontaneity of the binding of $\text{NO}_2\text{-H}_2\text{SALNN}$ with DNA by the negative ΔG° and positive ΔS° values. Simple synthesis procedure, low cost easily available starting materials and above all the clear and easy colorimetric sensing may offer the ligand enough prospects for large scale commercial use for the detection of methanol impurity in various foods and other beverages. The ability of the complex to displace nearly 93% of Hoechst 33258 from DNA opens another prospect as a substitute to some currently commercially available probes, such as Hoechst 33258 and DAPI.

Acknowledgement

US and MD thank Science & Engineering Research Board (SERB), Govt. of India for the award of National Post-doctoral fellowships (Ref. No.PDF/2016/000080 and Ref No.PDF/2016/000334).

References

- 1 P. Kumar, A. Deep, K.-H. Kima, and R.J.C. Brown, *Progress in Polymer Science*, 2015, **45**, 102–118.
- 2 M. Hakim, Y. Y. Broza, O. Barash, N. Peled, M. Phillips, A. Amann, and H. Haick, *Chem. Rev.* 2012, **112**, 5949–5966.
- 3 R. Atkinson *Atmos Environ* 2000, **34**, 2063–101.
- 4 G. Rowe, J.B. Hirsh and A.K. Anderson, *Proc Natl Acad Sci USA* 2007, **104**, 383–8.
- 5 K.S. Panday and H.K. Kim, *Environ Sci Technol*, 2009, **43**, 3020–9.
- 6 A.N. Martin, J.E. Leming, H.M. Henderson, P.R. Lipscombe, K.J. Black and D.S. Jarvis, *Atmos Environ* 2010, **44**, 3378–85.
- 7 I. Rahman, A. A. van Schadewijk, A. J. Crowther, P. S. Hiemstra, J. Stolk, W. MacNee and W. I. De Boer, *Am. J. Respir. Crit. Care Med.* 2002, **166**, 490.
- 8 L.S. Andrews, J.J. Clary, J.B. Terrill and H.F. Bolte, *J. Toxicol. Environ. Health*, 1987, **20**, 117–124.
- 9 J.W. Allis, B.L. Brown, J.E. Simmons, G.E. Hatch, A. McDonald and D.E. House, *Toxicology*, 1996, **112**, 131-170.
- 10 J. Wang, M. Jiang, L. Yan, R. Peng, M. Huangfu, X. Guo, Y. Li and P. Wu, *Inorg. Chem.* 2016, **55**, 12660–12668.
- 11 M. Tu and R.A. Fischer, *J Mater Chem A*, 2014, **2**, 2018–22.
- 12 M.D Allendorf, T.J.R Houk, L. Andruszkiewicz, A.A. Talin and J. Pikarsky, *J Am Chem Soc*, 2008, **130**, 14404–5.
- 13 N. G. Pramod, S. N. Pandey, P. P. Sahay, *Ceram. Int.* 2012, **38**, 4151–4158.
- 14 L. F. Song, C. H. Jiang, C. L. Jiao, J. A. Zhang, L. X. Sun, F. Xu, W. S. You, Z. G. Wang and J. J. Zhao, *Cryst. Growth Des.* 2010, **10**, 5020–5023.
- 15 M. Dolai, U. Saha, A. K. Das and G. S. Kumar, *Anal. Methods*, 2018, **10**, 4063-4072.
- 16 I. Chakraborty, U. Saha, R. Rakshit, S. Talukdar, G. Suresh Kumar and K. Mandal, *Materials Today Chemistry*, 2017, **5**, 92-100.
- 17 M. Inclán, M. T. Albelda, J. C. Frías, S. Blasco, B. Verdejo, C. Serena, C. S. -Canela, M. L. Díaz, A. G. -España and E. G. -España, *J. Am. Chem. Soc.*, 2012, **134**, 9644–9656.
- 18 S.H.V. Rijt and P.J. Sadler, *Drug Discov Today*, 2009, **14**, 1089-1097.
- 19 A. Basu, P. Jaisankar and G. S. Kumar, *Bioorg. Med. Chem.*, 2012, **20**, 2498-2505.
- 20 R. Bhowmick, A. S. M. Islam, U. Saha, G. S. Kumar and M. Ali, *New J. Chem.*, 2018, **42**, 3435-3443
- 21 C.V. Kumar and E.H. Asuncion, *J. Am. Chem. Soc.* 1993, **115**, 8547-8553
- 22 S. Udenfriend and P. Zaltzman, *Anal. Biochem.*, 1962, **3**, 49-59.
- 23 R. G. Parr and W. Yang, *Oxford University Press, Oxford*, 1989.
- 24 M. Cossi, N. Rega, G. Scalmani and V. Barone, *J. Comput. Chem.* 2003, **24**, 669-681.
- 25 A. D. Becke, *J. Chem. Phys.* 1993, **98**, 5648-5652.
- 26 W. Lee, W. Yang and R. G. Parr, *Phys. Rev. B*, 1998, **37**, 785-789.
- 27 R. Bauernschmitt and R. Ahlrichs, *Chem. Phys. Lett.*, 1996, **256** 454-464.
- 28 M. J. Frisch, G. W. Trucks, H. B. Schlegel, G. E. Scuseria, M. A. Robb, J. R. Cheeseman, G. Scalmani, V. Barone, B. Mennucci, G. A. Petersson, H. Nakatsuji, M. Caricato, X. Li, H. P. Hratchian, A. F. Izmaylov, J. Bloino, G. Zheng, J. L. Sonnenberg, M. Hada, M. Ehara, K. Toyota, R. Fukuda, J. Hasegawa, M. Ishida, T. Nakajima, Y. Honda, O. Kitao, H. Nakai, T. Vreven, J. A. Montgomery Jr., J. E. Peralta, F. Ogliaro, M. Bearpark, J. J. Heyd, E. Brothers, K. N. Kudin, V. N. Staroverov, R. Kobayashi, J. Normand, K. Raghavachari, A. Rendell, J. C. Burant, S. S. Iyengar, J. Tomasi, M. Cossi, N. Rega, J. M. Millam, M. Klene, J. E. Knox, J. B. Cross, V. Bakken, C. Adamo, J. Jaramillo, R. Gomperts, R. E. Stratmann, O. Yazyev, A. J. Austin, R. Cammi, C. Pomelli, J. W. Ochterski, R. L. Martin, K. Morokuma, V. G. Zakrzewski, G. A. Voth, P. Salvador, J. J. Dannenberg, S. Dapprich, A. D. Daniels, Ö. Farkas, J. B. Foresman, J. V. Ortiz, J. Cioslowski and D. J. Fox, *Gaussian Inc.*, 2009, *Wallingford CT*.
- 29 N. M. O'Boyle, A. L. Tenderholt and K. M. Langner, *J. Comp. Chem.* 2008, **29**, 839-845.
- 30 M. Dolai, U. Saha, G. Suresh Kumar and M. Ali, *ChemistrySelect*, 2018, **3**, 6935 – 6941.

- 1
2
3
4
5
6
7
8
9
10
11
12
13
14
15
16
17
18
19
20
21
22
23
24
25
26
27
28
29
30
31 K. Bhadra, M. Maiti and G. S. Kumar, *Biochim. Biophys. Acta* 2007, **1770**, 1071-1080.
32 A. Basu and G. S. Kumar, *J. Agric. Food Chem.*, 2014, **62**, 317-326.
33 H. A. Benesi and J. H. Hildebrand, *J. Am. Chem. Soc.* 1949, **71**, 2703-2707.
34 M. Dolai, U. Saha, G. Suresh Kumar, E. Zangrando and M. Ali, *Inorg. Chim. Acta*, 2018, **483**, 211-217.
35 M. Deiana, B. Mettra, K. Matczyszyn, K. Piela, D. Pitrat, J. Olesiak-Banska, C. Monnereau, C. Andraud and M. Samoc, *Phys. Chem. Chem. Phys.*, 2015, **17**, 30318.
36 A. Kunwar, E. Simon, U. Singh, R. K. Chittela, D. Sharma, S. K. Sandur and I. K. Priyadarsini, *Chem. Biol. Drug Des.*, 2011, **77**, 281.
37 S. Arunaguiri and B. G. Maiya, *Inorg. Chem.*, 1999, **38**, 842-843.
38 B. K. Sahoo, K. S. Ghosh, R. Bera and S. Dasgupta, *Chemical Physics*, 2008, **351**, 163-169.
39 P.E. Pjura, K. Grzeskowiak and R.E. Dickerson, *J. Mol. Biol.*, 1987, **197**, 257.

TOC

Adaptable sensor for paying fluorometric detection of methanol molecules: theoretical aspects and DNA binding studies

Urmila Saha^{a,*}, Malay Dolai^b and Gopinatha Suresh Kumar^a

